Journal of the Brazilian Society of Mechanical Sciences and Engineering (2019) 41:356
https://doi.org/10.1007/s40430-019-1852-2

TECHNICAL PAPER

Numerical study of a waste heat recovery thermogenerator system

P. Donoso-García[1] · **L. Henríquez-Vargas**[1]

Received: 22 October 2018 / Accepted: 24 July 2019 / Published online: 8 August 2019
© The Brazilian Society of Mechanical Sciences and Engineering 2019

Abstract

This paper presents a numerical study on waste heat recovery from a fluid stream using thermoelectric elements for energy harvesting. Two fluids were tested, air and steam, and the voltage and overall efficiency were computed for different sets of operational conditions. The mathematical description considered turbulent regime and coupled transport phenomena for the description of the main thermoelectric effects. Numerical solution was achieved using ANSYS/FLUENT commercial software with complementary implementations of user-defined scalars and user-defined functions to account for the mathematical model specific needs. The system global efficiency was computed for a pair of heat extraction conditions and different operational variables giving values within [0.11–9.22] (%). It was found that the global efficiency increases with the fluid temperature and the decrease in the external thermal resistance. For all cases studied, the global efficiency was greater when air was used as a heat carrier fluid due to its specific heat values which were about half the steam ones.

Keywords Waste heat · Thermoelectricity · Heat recovery · Seebeck effect

List of symbols

c_p	Specific heat capacity
$c_{1\varepsilon}$	Turbulent model parameter
$c_{2\varepsilon}$	Turbulent model parameter
c_μ	Turbulent model parameter
$\mathbf{D}$	Mass transport tensor
D	Square duct side
D	Mass diffusivity
$\mathbf{E}$	Electric field intensity vector
e	Height
$\mathbf{g}$	External field acceleration
G_k	Rate of k generation
H	Specific enthalpy
h	Heat transfer coefficient
$\mathbf{I}$	Unitary tensor
I	Current
$\mathbf{J}$	Electric current density vector
$\mathbf{K}$	Effective conductivity tensor
k	Turbulent kinetic energy
L	Length
$\dot{m}$	Mass flow
M	Molar weight
m	Mass fraction
N_n	Number of thermoelectric elements
p_0	Pressure
P	Power
Pr	Prandtl number
$\boldsymbol{q}$	Total heat flux vector
$\dot{q}$	Heat generation per unit volume
Q_C	Heat outflow from cold reservoir
Q_H	Heat inflow from hot reservoir
$\bar{R}$	Universal gas constant
R_C	Heat resistance at cold junction
R_e	Electrical resistance
R_H	Heat resistance at hot junction
S	Generic source term
Sc	Schmidt number
T	Temperature
t	Time
$\mathbf{u}_\mathrm{D}$	Gas velocity
W	Width

Subscripts

0	Inlet
B	Bottom
C	Center
Ce	Relative to ceramic phase

Technical Editor: Jader Barbosa Jr.

✉ P. Donoso-García
pablo.donosoga@usach.cl

L. Henríquez-Vargas
luis.henriquez@usach.cl

[1] Chemical Engineering Department, Universidad de Santiago, B. O'Higgins #3363, Santiago, Chile

Cu	Relative to the copper phase
E	Relative to electricity conducting phases
eff	Effective
f	Relative to fluid phase
i	Internal
I	Interspacing between thermoelectric legs
L	Outlet
L	Left
max	Maximum
min	Minimum
n	Relative to n-type semiconductor phase
norm	Normalized variable
o	External
p	Relative to p-type semiconductor phase
R	Right
s	Relative to solid phase
T	Top
t	Turbulent

Greek

$\boldsymbol{\alpha}$	Absolute Seebeck coefficient tensor
$\boldsymbol{\Gamma}$	Generic transport property tensor
ε	Rate of dissipation of k
η	Global efficiency
λ	Thermal conductivity
μ	Dynamic viscosity
$\boldsymbol{\xi}$	Permittivity tensor
ρ	Density
$\boldsymbol{\sigma}$	Electric conductivity tensor
σ_ε	Turbulent model parameter
σ_k	Turbulent model parameter
$\overline{\overline{\boldsymbol{\tau}}}$	Turbulent and molecular stress tensor
φ	Generic transported quantity
ψ	Voltage

1 Introduction

Much of the energy generated today is dissipated to the environment, wasting heat from different industrial sectors. The sustained increase in demand for electricity and the environmental impact of current generation systems have required the study of potential methods for more efficient energy production and optimization of existing mechanisms.

Thermoelectric generation technology can directly transform thermal energy into electricity by using thermoelectric transformation materials. A thermoelectric power converter has no moving parts, and is compact, quiet, highly reliable and environmentally friendly [13]. Owing to these advantages, there has been considerable emphasis on the development of small thermoelectric generators for a variety of aerospace and military applications over the past years [4]. More recently, there is a growing interest for waste heat recovery thermoelectric generator, using various heat sources such as combustion of solid wastes, geothermal energy, power plants and other industrial heat-generating processes [21].

Power generation from waste heat streams using thermoelectric materials has been overlooked due to its low thermal efficiencies ($\sim 4(\%)$) [6]. In the case of a waste heat thermoelectric generator (TEG), there have been many conceptual designs of a power conversion system which is potentially capable of being applied in this field [4, 5, 14, 17, 21–23, 27, 28]. For waste heat recovery and subsequent conversion into electricity, it has been used prototypes that used clear fluids and thermoelectric devices, present in many daily industrial processes. An experimental TEG prototype, including a counterflow heat exchanger, was studied in [26], revealing the existence of a direct relationship between the output power and the fluid mass flow rate. In this field, using the thermoelectric effect under different operating conditions and manufacturing material for modules, with an installed power of 1 (kW) and 500 (W), it was established that the cost of the TEG is lower than a photovoltaic system, in terms of an equivalent amount of energy generated [19, 20]. These specific advantages make this type of waste heat recovery technology an option that can still be improved in terms of thermoelectric efficiency, which can contribute to the decrease in fossil fuels consumption thus lowering the environmental impact.

Extensive studies on the topic have generated a solid knowledge base for the main characteristics of this type of thermoelectric generators. However, the vast majority of these numerical studies have developed for waste heat extraction systems without considering turbulent transport and the benefits that it could generate.

2 System description

The system under study consists of a portion of a metal square duct with side D and axis segments L_L, L_C and L_R, within which a waste heat carrier fluid, such as steam or air, flows. This selection of materials is because they are the most commonly transported work fluids alongside with water found in multiple industrial applications. In the present study, we considered, steam and air, due to the higher temperatures that can be found using these working fluids in industrial operations.

In the flow section, the fluid enters with velocity $\mathbf{u}_{D0}$ and temperature T_{f0}. On the outer mantle, N_{TE} thermoelectric devices have been arranged electrically in series and are confined between a ceramic material that isolates them electrically, as shown in Fig. 1. This structural arrangement allows the recovery of residual thermal energy from the fluid, passing this heat to the thermoelements generating an electric potential $\Delta\psi$ due to the Seebeck effect.

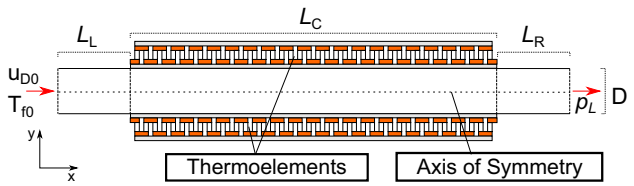

Fig. 1 Reactor scheme with heat recovery system and thermoelectric modules

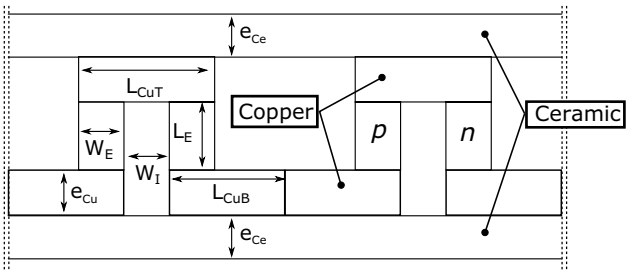

Fig. 2 Thermoelectric modules scheme

The basic thermoelectric unit is formed by a pair of semiconductor materials, type *n* and *p*, whom are electrically connected by copper electrodes. The heat transfer rate is controlled by a ceramic material plate since typically the semiconductor has an upper thermal operational limit at ≈ 400 (°C), see Fig. 2. The present study is an extension of a previous publication by the authors [11, 12] that considered turbulent reactive flow in porous media, recuperative reactor and thermogeneration. In the present work, we considered 2D plane geometry with variations in the type of fluid carrying residual energy, operational variables and heat extraction conditions.

3 Mathematical model

The governing equations necessary to describe the turbulent transport of momentum and energy for a clear fluid and the transfer of energy to its enclosing walls include

The ideal gas law

$$\rho_{\mathrm{f}} = \frac{p_0}{\bar{R} T_{\mathrm{f}} \sum \frac{m_i}{M_i}} \tag{1}$$

where $\bar{R}$ is the universal gas constant, p the operating pressure, m_i and M_i are the mass fraction and the molecular weight of species i, respectively.

Continuity equation

$$\frac{\partial}{\partial t}\left(\rho_{\mathrm{f}}\right) + \nabla \cdot \left(\rho_{\mathrm{f}} \mathbf{u}_{\mathrm{D}}\right) = 0 \tag{2}$$

where t is time and $\mathbf{u}_{\mathrm{D}}$ is the velocity vector.

Fluid phase energy equation

$$\frac{\partial}{\partial t}\left(\rho_{\mathrm{f}} c_{pf} T_{\mathrm{f}}\right) + \nabla \cdot \left(\rho_{\mathrm{f}} \mathbf{u}_{\mathrm{D}} c_{pf} T_{\mathrm{f}}\right) = \nabla \cdot \left(\mathbf{K}_{\mathrm{eff,f}} \cdot \nabla T_{\mathrm{f}}\right) \tag{3}$$

with, c_{pf} is fluid heat capacity, and $\mathbf{K}_{\mathrm{eff,f}}$ is the effective conductivity tensor for the fluid phase.

Solid phase energy equation

$$\frac{\partial}{\partial t}\left(\rho_{\mathrm{s}} c_{ps} T_{\mathrm{s}}\right) = \nabla \cdot \left(\mathbf{K}_{\mathrm{eff,s}} \cdot \nabla T_{\mathrm{s}}\right) \tag{4}$$

where ρ_{s} is the density, c_{ps} is the heat capacity and $\mathbf{K}_{\mathrm{eff,s}}$ is the effective conductivity tensor for the solid phase.

Macroscopic turbulent flow momentum equation

$$\frac{\partial}{\partial t}\left(\rho_{\mathrm{f}} \mathbf{u}_{\mathrm{D}}\right) + \nabla \cdot \left(\rho_{\mathrm{f}} \mathbf{u}_{\mathrm{D}} \mathbf{u}_{\mathrm{D}}\right) = -\nabla p + \nabla \cdot \left(\bar{\bar{\tau}}\right) + \rho_{\mathrm{f}} \mathbf{g} \tag{5}$$

with $\bar{\bar{\tau}}$ the molecular and turbulent stress tensor.

Turbulent kinetic energy and its rate of dissipation equations

$$\frac{\partial}{\partial t}\left(\rho_{\mathrm{f}} k\right) + \nabla \cdot \left(\rho_{\mathrm{f}} \mathbf{u}_{\mathrm{D}} k\right) = \nabla \cdot \left[\left(\mu + \frac{\mu_{\mathrm{t}}}{\sigma_k}\right) \nabla k\right] + G_k - \rho_{\mathrm{f}} \varepsilon \tag{6}$$

$$\frac{\partial}{\partial t}\left(\rho_{\mathrm{f}} \varepsilon\right) + \nabla \cdot \left(\rho_{\mathrm{f}} \mathbf{u}_{\mathrm{D}} \varepsilon\right) = \nabla \cdot \left[\left(\mu + \frac{\mu_{\mathrm{t}}}{\sigma_\varepsilon}\right) \nabla \varepsilon\right] + c_{1\varepsilon} \frac{\varepsilon}{k} G_k - c_{2\varepsilon} \rho_{\mathrm{f}} \frac{\varepsilon^2}{k} \tag{7}$$

with G_k represent the turbulent kinetic energy generation due to the mean velocity gradients, μ_{t} is the turbulent viscosity computed as follows

$$\mu_{\mathrm{t}} = c_\mu \rho_{\mathrm{f}} \frac{k^2}{\varepsilon} \tag{8}$$

here σ_k, σ_ε, $c_{1\varepsilon}$, $c_{2\varepsilon}$ and c_μ are dimensionless constants.

The boundary conditions considered were

$$\begin{aligned} &x = 0 \\ &\mathrm{u}_{\mathrm{D}} = \mathrm{u}_{\mathrm{D0}}, \quad T_{\mathrm{f}} = T_0, \quad k = k_0, \quad \varepsilon = \varepsilon_0 \end{aligned} \tag{9}$$

$$\begin{aligned} &x = \mathrm{L} \\ &\nabla T_{\mathrm{f}} = \nabla k = \nabla \varepsilon = 0, \quad p = p_L \end{aligned} \tag{10}$$

at walls no-slip velocity condition was established. The standard wall functions were used for turbulent variables treatment near the wall [1, 30]. In the inlet and outlet domain, the specification method of transported turbulence quantities intensity and viscosity ratio was implemented. On the axis, the boundary conditions include zero normal velocity and zero normal gradients of all variables in the symmetry plane.

The physical properties of air are computed using the following correlations [15].

$$c_{pf} = 947.0\, e^{1.83\times10^{-4} T_{\mathrm{f}}} \tag{11a}$$

$$\lambda_{\mathrm{f}} = 4.82 \times 10^{-7} c_{pf} T_{\mathrm{f}}^{0.7} \tag{11b}$$

$$\mu_{\mathrm{f}} = 3.37 \times 10^{-7} T_{\mathrm{f}}^{0.7} \tag{11c}$$

The physical properties of the steam are calculated using exponential adjustments to the data series in the temperature range 400–600 (K), presented in [29]. The deviation in the prediction of the physical properties is in the order of [0.005–1.5] (%).

$$c_{pf} = 1780.3\, e^{2.89\times10^{-4} T_{\mathrm{f}}} \tag{12a}$$

$$\lambda_{\mathrm{f}} = 1.01 \times 10^{-2} e^{2.39\times10^{-3} T_{\mathrm{f}}} \tag{12b}$$

$$\mu_{\mathrm{f}} = 5.754 \times 10^{-5} e^{2.15\times10^{-3} T_{\mathrm{f}}} \tag{12c}$$

The effective thermal conductivity and diffusivity included molecular and turbulent transport

$$\lambda_{\mathrm{eff,f}} = \lambda_{\mathrm{f}} + \frac{c_{pf}\mu_{\mathrm{t}}}{\mathrm{Pr}_{\mathrm{t}}} \tag{13}$$

$$D_{\mathrm{eff,f}} = D_{\mathrm{f}} + \frac{\mu_{\mathrm{t}}}{\rho_{\mathrm{f}} \mathrm{Sc}_{\mathrm{t}}} \tag{14}$$

where D_{f} is the molecular mass transport coefficient, Pr_{t} is the turbulent Prandtl number, and Sc_{t} is the turbulent Schmidt number. The last two latter were taken as constant [1].

The fluid and solid phases effective transport properties tensors are given by

$$\mathbf{D}_{\mathrm{eff,f}} = \left[D_{\mathrm{eff,f}}\right]\mathbf{I} \tag{15a}$$

$$\mathbf{K}_{\mathrm{eff,f}} = \left[\lambda_{\mathrm{eff,f}}\right]\mathbf{I} \tag{15b}$$

$$\mathbf{K}_{\mathrm{eff,s}} = \left[\lambda_{\mathrm{eff,s}}\right]\mathbf{I} \tag{15c}$$

It should be noted that for the effective transport properties and their respective tensors, the subscript f is modified by the one corresponding to the air or steam, as appropriate.

3.1 Thermoelectric generation

Modeling the thermoelectric generation phenomenon in solids (TEG) is based on the theory of non-equilibrium thermodynamics [7–9]. The modeling approach includes the solution of the equations of conservation of energy and conservation of charge in each of the thermoelectric devices and the coupled transport phenomena which gives origin to the Seebeck effect among others. The equations used in this work correspond to the form proposed by Antonova and Looman [3].

The equation of energy for the solid phase is

$$\frac{\partial}{\partial t}\rho\left(\rho_{\mathrm{E}} c_{p\mathrm{E}} T_{\mathrm{E}}\right) = \nabla \cdot \boldsymbol{q} + \dot{q} \tag{16}$$

with ρ_{E} the density, $c_{p\mathrm{E}}$ the heat capacity, T_{E} the temperature, $\boldsymbol{q}$ the total heat flux vector including the Peltier effect and $\dot{q}$ the heat generation rate due to the Joule effect and work done against the Seebeck electric field.

The continuity of charge is expressed by the following equation

$$\nabla \cdot \left(\boldsymbol{J} + \frac{\partial \mathbf{D}}{\partial t}\right) = 0 \tag{17}$$

where $\boldsymbol{J}$ is the electric current density vector and $\mathbf{D}$ is the electric flux density vector.

The constitutive relations and final form of the heat generation term are

$$\boldsymbol{q} = T\boldsymbol{\alpha}_{\mathrm{E}} \cdot \boldsymbol{J} - \mathbf{K}_{\mathrm{E}} \cdot \nabla T \tag{18}$$

$$\boldsymbol{J} = \boldsymbol{\sigma}_{\mathrm{E}} \cdot \left(\mathbf{E} - \boldsymbol{\alpha}_{\mathrm{E}} \cdot \nabla T\right) \tag{19}$$

$$\mathbf{D} = \boldsymbol{\xi} \cdot \mathbf{E} \tag{20}$$

$$\mathbf{E} = -\nabla \psi \tag{21}$$

$$\dot{q} = \boldsymbol{J}^2 / \boldsymbol{\sigma}_{\mathrm{E}} \tag{22}$$

with $\boldsymbol{\sigma}_{\mathrm{E}}$ the electric conductivity tensor, $\boldsymbol{\alpha}_{\mathrm{E}}$ the Seebeck coefficient tensor, $\mathbf{K}_{\mathrm{E}}$ the thermal conductivity tensor, $\boldsymbol{\xi}$ the permittivity tensor and ψ the voltage.

The governing equations will be expressed in its extended form by combining the energy and charge equations with the constitutive relations, resulting in the expressions 23 and 24 for the conservation of energy and charge, respectively.

$$\begin{aligned}\frac{\partial}{\partial t}\left(\rho_{\mathrm{E}} c_{p\mathrm{E}} T_{\mathrm{E}}\right) = {} & \nabla \cdot \left[\left(\boldsymbol{\sigma}_{\mathrm{E}} \cdot \boldsymbol{\alpha}_{\mathrm{E}}^2 T_{\mathrm{E}} + \mathbf{K}_{\mathrm{E}}\right) \cdot \nabla T_{\mathrm{E}}\right] \\ & + \boldsymbol{\sigma}_{\mathrm{E}} \cdot \left[(\nabla\psi)^2 + 2\boldsymbol{\alpha}_{\mathrm{E}} \cdot \nabla T_{\mathrm{E}} \cdot \nabla\psi + \left(\boldsymbol{\alpha}_{\mathrm{E}} \cdot \nabla T_{\mathrm{E}}\right)^2\right] \\ & + \nabla \cdot \left(\boldsymbol{\sigma}_{\mathrm{E}} \cdot \boldsymbol{\alpha}_{\mathrm{E}} T_{\mathrm{E}} \cdot \nabla\psi\right)\end{aligned} \tag{23}$$

$$\nabla \cdot \left(\boldsymbol{\xi} \cdot \nabla \frac{\partial \psi}{\partial t}\right) + \nabla \cdot \left(\boldsymbol{\sigma}_{\mathrm{E}} \cdot \boldsymbol{\alpha}_{\mathrm{E}} \cdot \nabla T_{\mathrm{E}}\right) + \nabla \cdot \left(\boldsymbol{\sigma}_{\mathrm{E}} \cdot \nabla\psi\right) = 0 \tag{24}$$

In Fig. 3, thermoelectric elements connected electrically in series are shown. Thermoelectric elements are essentially devices operating between reservoirs of high temperature and a low temperature, where Q_H and Q_C represent their respective heat flows.

Using the relation given by the extended Ohm's Law [16], the electric current intensity can be determined from the following equation

$$I = \frac{\boldsymbol{\alpha}_p \cdot \sum_{i=1}^{Nn} \Delta T_{p,i} - \boldsymbol{\alpha}_n \cdot \sum_{i=1}^{Nn} \Delta T_{n,i}}{\left(1 + R_{e,o}^{*}\right) \sum_{i=1}^{Nn} R_{e,i}} \tag{25}$$

where ΔT_p and ΔT_n are temperature differences in the semiconductor p and n, respectively. $R_{e,i}$ is the internal electrical

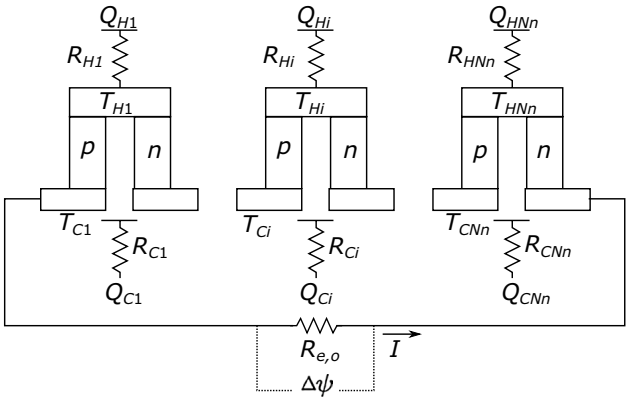

Fig. 3 Scheme *Nn* thermocouples electrically connected in series [10]

resistance, and $R^*_{e,o}$ is the internal to external electrical resistance ratio. For a maximum power output, $R^*_{e,o} = 1$ must be set [24].

The overall efficiency of the process is defined as the generated electric power over the fluid enthalpy change times the mass flow rate

$$\eta = \frac{\mathrm{P}}{\dot{m}\left(H_0 - H_L\right)} = \frac{I^2\left(\sum_{i=1}^{Nn} R_{e,i} + R_{e,o}\right)}{\mathrm{D}^2\ \mathbf{u}_{\mathrm{D0}}\rho_{\mathrm{f0}}\left(H_0 - H_L\right)} \tag{26}$$

$$\eta = \frac{I^2 N_n R_{e,i}(1 + R^*_{e,o})}{\mathrm{D}^2\ \mathbf{u}_{\mathrm{D0}}\ \rho_{\mathrm{f0}}\ \overline{c}_{p\mathrm{f}}\ \Delta T_{\mathrm{f}}} \tag{27}$$

with $R_{e,o}$ external electrical resistance, H fluid specific enthalpy.

4 Numerical method

The standard FLUENT interface does not cover all the modeling needs of the user. Complementary, the software provides two extensions for modeling purposes in the form of user-defined functions (UDF) and user-defined scalars (UDS). The former allows for customization of boundary conditions, source terms, reaction rates, physical properties, among others, while the latter can be used to solve generic transport equations for arbitrary scalars φ in the form [2]

$$\frac{\partial}{\partial t}(\rho\varphi) + \nabla \cdot \left(\rho\mathbf{u}_{\mathrm{D}}\varphi - \boldsymbol{\Gamma} \cdot \nabla\varphi\right) = S \tag{28}$$

where $\boldsymbol{\Gamma}$ and S are the diffusion tensor and the source term, respectively, which must be defined for each scalar equation.

We implement the equations set for estimation of physical properties, Eqs. 11 – 12 and the voltage related source terms in Eq. 23, in the form of UDFs. The conservation of electric charge, Eq. 24, was incorporated into the FLUENT solver through the use of UDS.

The system of differential equations was discretized with the finite volume method with upwind scheme for convective terms, and pressure–velocity coupling is solved using the SIMPLE algorithm for incompressible fluid [1, 25].

Thermoelectric model validation was conducted replicating the results of Jaegle [18] and were presented by the authors in a previous publication [12].

The model was solved using axial symmetry, and, based on the complexity of the phenomena to be modeled, differential meshing was performed by region. The input channel was discretized with a size equal to 2×10^{-3} (m), whereas element sizes were 5.0×10^{-4} (m) in the thermoelectric region. A good compromise between accuracy and computation time was found with the grid size of ~ 80.000 elements.

All simulations were based on the standard parameters presented in Table 1.

Table 1 Standard case values

Symbol	Dimension	Value
e_{Cu}	m	1.0×10^{-3}
e_{Ce}	m	1.0×10^{-3}
W_{E}	m	2.0×10^{-3}
W_{I}	m	2.0×10^{-3}
L_{CuT}	m	4.0×10^{-3}
L_{CuB}	m	4.0×10^{-3}
L_{E}	m	1.0×10^{-3}
D	m	0.05
L_{L}	m	0.07
L_{C}	m	0.12
L_{R}	m	0.07
N_n	Dimensionless	20
$R^*_{e,o}$	Dimensionless	1
T_0	K	300
h	W/m^2 K	20
p_0	Pa	101,325
c_μ	Dimensionless	0.09
$c_{1\epsilon}$	Dimensionless	1.44
$c_{2\epsilon}$	Dimensionless	1.92
σ_k	Dimensionless	1.0
σ_ϵ	Dimensionless	1.3
$\mathrm{Pr_t}$	Dimensionless	0.85
$\mathrm{Sc_t}$	Dimensionless	0.7

5 Results and discussion

The fluid flows through the interior of the duct and yields sensible heat to the thermoelectric devices attached to the mantle only in the solid–fluid interface. Due to the Seebeck effect, an electric potential is generated and the fraction of heat not converted into electricity is rejected to the surroundings. Two heat transfer coefficients were used to analyze their influence on heat conversion to electricity, h and $h' = 100h$. Different values of inlet velocity $\mathbf{u}_{D0} = [1, 2, 3]$ (m/s) and incoming fluid temperature $T_{f0} = [400, 450, 500, 550, 600]$ (K) were used to study the residual heat recovery. Normalized values of electric potential, efficiency and power will be presented in the form

$$\eta_{norm} = \frac{\eta - \eta_{\min}}{\eta_{\max} - \eta_{\min}} \tag{29}$$

$$\Delta\psi_{norm} = \frac{\Delta\psi - \Delta\psi_{\min}}{\Delta\psi_{\max} - \Delta\psi_{\min}} \tag{30}$$

$$\mathrm{P}_{norm} = \frac{\mathrm{P} - \mathrm{P}_{\min}}{\mathrm{P}_{\max} - \mathrm{P}_{\min}} \tag{31}$$

where the min and max subindexes refer to the minimum and maximum values for the complete set of results.

Figures 4 and 5 show the variation of electric potential as function of the operational variables ($\mathbf{u}_{D0}$, T_{f0}) and the different conditions of heat extraction (h, h'), for air and steam, respectively.

The electric potential is determined by solving the coupled equations of electric charge conservation and thermal energy balance within the thermoelectric elements domain, see Sect. 3.1. At one end of the electrical circuit, it is imposed ground voltage condition, while at the other end, it is imposed an estimation of the electric current by Eq. 25. Under the initial heat extraction conditions, it was found that the values of $\Delta\psi$ increase with the fluid thermal load, reaching values within [34.11–105.02] (mV) and [33.93–104.38] (mV) for air and steam, respectively. The electric potential values obtained are of similar magnitude due to the similar thermal conductivity values of both fluids within the temperature range studied. The similarity in the values of this transport property generates equivalent heat transfer rates at the fluid–solid interface, which cause a homogeneous temperature distribution in the thermoelectric devices, as shown in Fig. 6. This temperature distribution between the ends of the thermoelements results in a generation of an electric potential due to the Seebeck effect which can be seen from Fig. 7. Considering the heat

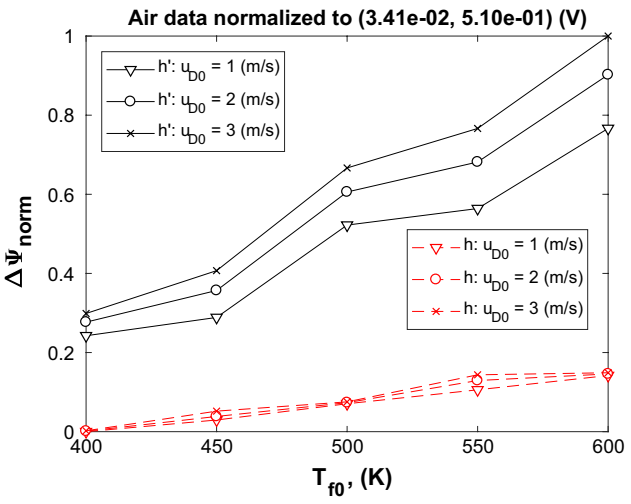

Fig. 4 Voltage obtained for air

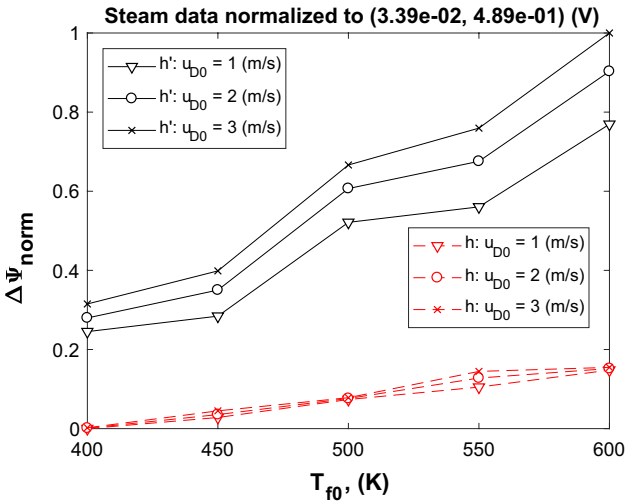

Fig. 5 Voltage obtained for steam

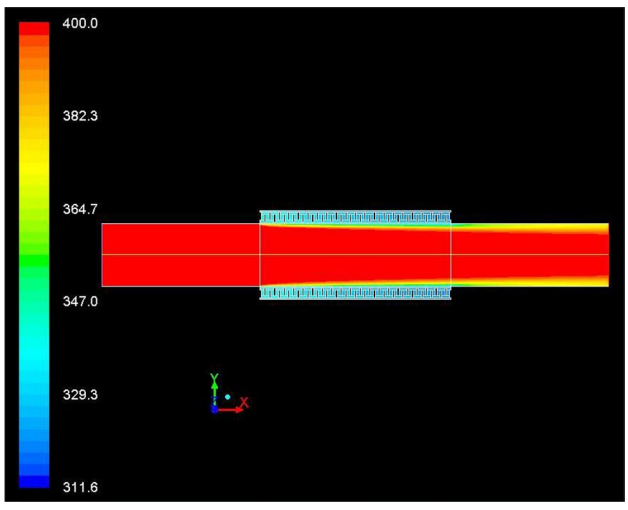

Fig. 6 Temperature contours in (K) obtained for $\mathbf{u}_{D0} = 1$ (m/s) and $T_{f0} = 400$ (K) with steam as waste heat carrier fluid

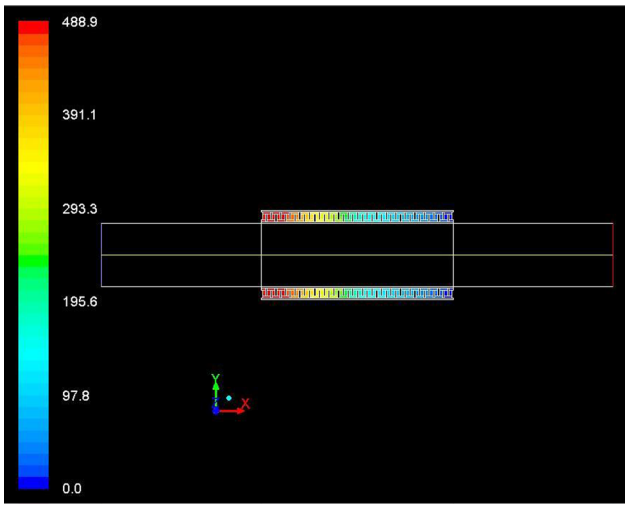

Fig. 7 Voltage contours $\Delta\psi'$ in (mV) obtained for $\mathbf{u}_{D0} = 3$ (m/s) and $T_{f0} = 600$ (K) with steam as waste heat carrier fluid

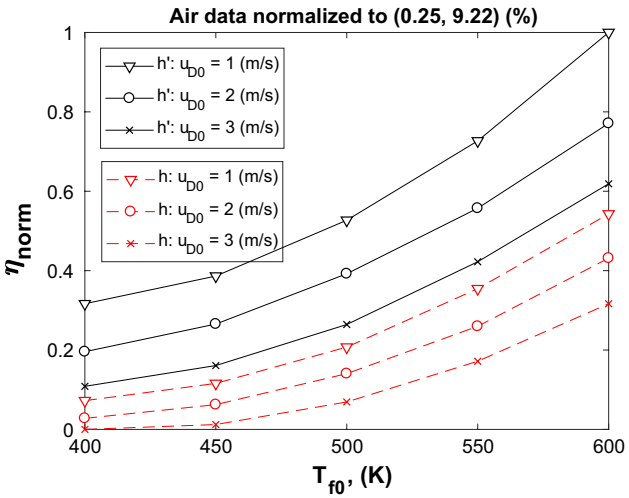

Fig. 8 Overall efficiency values for air

transfer coefficient h', the new values of $\Delta\psi'$ are within [164.25–510.28] (mV) and [159.52–488.87] (mV) for air and steam, respectively. The increase in these values lies within the range of [4.68–4.85] times the determined values when the heat transfer coefficient was h. From these results, it can be stated that the thermoelectric generation under the system considered for study is favored with the increase in the working fluid thermal load, being further accentuated with the increase in the heat extraction rate at the ceramic material upper boundary.

Overall efficiency is directly proportional to the product of the square of the electrical current and the electrical resistance and inversely proportional to the energy delivered by the waste heat carrier fluid, as expressed in Eq. 27. The efficiency values increase with the fluid temperature, together with a thermal resistance decrease for the energy flow to the environment, because higher thermal gradients favor thermogeneration and conversion efficiency, as shown in Figs. 8 and 9. For the initial conditions of heat extraction, it was found that the values of η are within [0.25–5.12] (%) and [0.11–4.28] (%) for air and steam, respectively, while with the heat transfer coefficient h', values of η' fall within [1.55–9.22] (%) and [1.22–7.68] (%), for air and steam, respectively. It is noted that the overall efficiency values decrease with the increase in the fluid thermal load. With reference to Eq. 27, the electric current increase is not proportional to the energy input increase. Consequently, the overall energy efficiency decreases with higher thermal loads of the residual energy carrier fluid. Under equivalent operating conditions, the efficiency was higher when air was used as the carrier fluid. This response is due to the specific heat values computed from Eqs. 11 and 12. Using the average temperature of each fluid, for the set of cases studied, it was found that the value of the specific heat of the steam doubles the air one, thus promoting lower values of global efficiency. Temperature drop values were found in the range [0.31–15.75] (K) and [0.13–15.14] (K), for air and steam, respectively, with the higher values obtained with the decrease in the heat resistance and the gas velocity.

Power was calculated from the product between the square of the current intensity and the total electrical resistance of thermogenerator system. Figures 10 and 11 present the total power obtained from the computational predictions. The values of P under the initial conditions of heat extraction increase slightly as the thermal load of the fluids also increases, reaching values of [0.03–0.31] (W) and [0.03–0.30] (W) for air and steam, respectively, while, when the heat extraction conditions were modified the P′ values

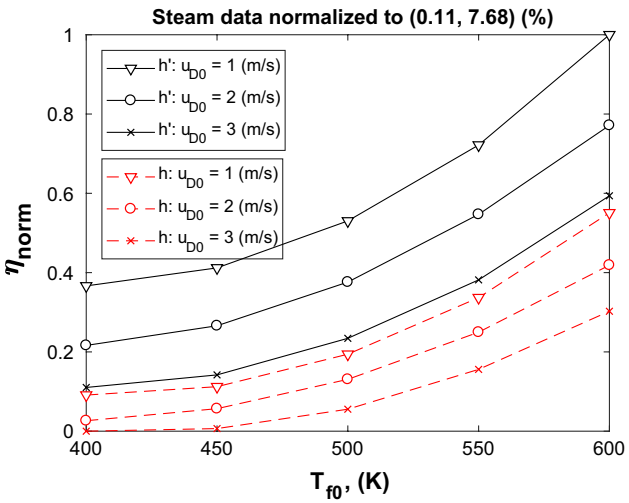

Fig. 9 Overall efficiency values for steam

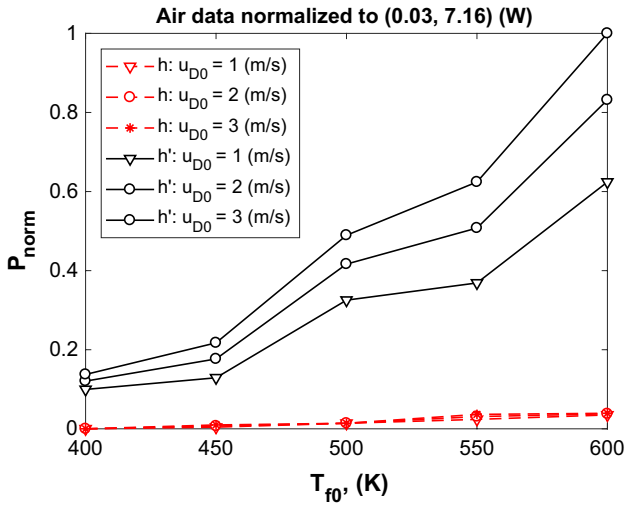

Fig. 10 Power obtained for air

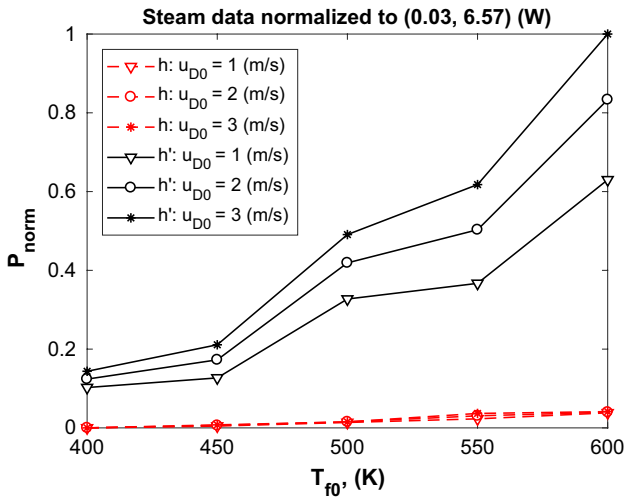

Fig. 11 Power obtained for steam

reached [0.74–7.16] (W) and [0.70–6.57] (W). The increase in these values is within the range of [14.2–29.6] times the values determined when the coefficient implemented was h. The calculated values of P and P′ are consistent with the evolution of $\Delta\psi$ presented in Figs. 4 and 5, since Ohm's Law establishes a direct proportionality of the power with the square of the voltage, which is reflected in the high peak of P′ with the increase of $\Delta\psi$.

6 Conclusions

A numerical study on waste heat recovery system and energy conversion by thermoelectric generator was performed.

Under the range of variables tested, the highest values of electrical potential were reached when the thermal load of the working fluids was increased. It was observed that lower heat transfer resistance values to the environment produce higher temperature gradients in the thermoelectric devices and consequently increase the electrical potential due to the Seebeck effect.

The overall efficiency increased with the inlet temperature of the fluids and decreased with their thermal load. The highest efficiency values were reached when the thermal resistance was decreased and the residual energy carrier fluid was air. This was due to the fact that the value of the specific heat of the gas was approximately half of the value of the same intensive property of the steam within the operational conditions considered.

As presented, the external coupling of the TEG system is an alternative method for residual energy harvesting without the need of complex internal structures which may cause perturbations in the flow field. In operational terms, the temperature drop generated by the heat extraction is not enough to generate steam or air condensation up to a ≈ 80 (%) of relative humidity.

Acknowledgements The authors wish to acknowledge DICYT project 091611DG.

References

1. ANSYS: ANSYS FLUENT theory guide, release 14.5 (2011)
2. ANSYS: ANSYS FLUENT UDF manual, release 14.5 (2011)
3. Antonova EE, Looman DC (2005) Finite elements for thermoelectric device analysis in ANSYS. In: International conference on thermoelectrics
4. Basel I, Ahmed H (2009) Thermoelectric power generation using waste-heat energy as an alternative green technology. Rec Patents Electr Eng 2:27–39
5. Beeby S, White N (2010) Energy harvesting for autonomous systems, 1st edn. Artech House, London
6. Crane DT, Jackson GS (2004) Optimization of cross flow heat exchangers for thermoelectric waste heat recovery. Energy Convers Manag 45:1565–1582
7. Domenicali C (1953) Irreversible thermodynamics of thermoelectric effects in inhomogeneous anisotropic media. Phys Rev 92(4):877–881
8. Domenicali C (1954) Irreversible thermodynamics of thermoelectricity. Rev Mod Phys 26(2):237–275
9. Domenicali C (1954) Stationary temperature distribution in an electrically heater conductor. J Appl Phys 25(10):1310–1311
10. Donoso García P (2011) Estudio de la Termogeneración de electricidad por combustión en medios porosos inertes. Ph.D. Thesis, Universidad de Santiago de Chile
11. Donoso-García P, Henríquez-Vargas L (2016) Numerical study of porous media turbulent combustion in a recuperative reactor. J Porous Media 19(11):941–953. https://doi.org/10.1615/JPorMedia.v19.i11.20
12. Donoso-García P, Henríquez-Vargas L (2015) Numerical study of turbulent porous media combustion coupled with thermoelectric

generation in a recuperative reactor. Energy 93:1189–1198. https://doi.org/10.1016/j.energy.2015.09.123
13. Gou X, Xiao H, Yang S (2010) Modeling, experimental study and optimization on low-temperature waste heat thermoelectric generator system. Appl Energy 87:3131–3136
14. Hendricks T, Choate W (2006) Engineering scoping study of thermoelectric generation systems for industrial waste heat recovery
15. Henríquez-Vargas L, Bubnovich V, Cubillos F, Donoso P (2013) Modeling, simulation and control for a continuous porous media burner. J Porous Media 16(2):155–165. https://doi.org/10.1615/JPorMedia.v16.i2.60
16. Henríquez-Vargas L, Loyola J, Sanhueza D, Donoso P (2015) Numerical study of reciprocal flow porous media burners coupled with thermoelectric generation. J Porous Media 18(3):257–267. https://doi.org/10.1615/JPorMedia.v18.i3.60
17. Hsu CT, Huang GY, Chu HS, Yu B, Yao DJ (2011) Experiments and simulations on low-temperature waste heat harvesting system by thermoelectric power generators. Appl Energy 88:1291–1297
18. Jaegle M (2008) Multiphysics simulation of thermoelectric systems. In: Comsol conference
19. Liu C, Chen P, Li K (2014) A 1 kW thermoelectric generator for low-temperature geothermal resources. In: Proceedings, thirty-ninth workshop on geothermal reservoir engineering, SGP-TR-202, February 24–26
20. Liu C, Chen P, Li K (2014) A 500 W low-temperature thermoelectric generator: design and experimental study. Int J Hydrog Energy 39:15497–15505
21. Niu X, Yu J, Wang S (2009) Experimental study on low-temperature waste heat thermoelectric generator. Power Sources 188:621–626
22. Ofoegbu C, Mazumder S (2015) Computational modeling of a solar thermoelectric generator. J Therm Sci Eng Appl 7:041004-1–041004-7
23. Orr B, Akbarzadeh A, Mochizuki M, Singh R (2016) A review of car waste heat recovery systems utilising thermoelectric generators and heat pipes. Appl Therm Eng 101:490–495
24. Park C, Kaviany M (2000) Combustion-thermoelectric tube. Heat Transf 122:721–729
25. Patankar S (1980) Numerical heat transfer and fluid flow, 1st edn. Hemisphere Publishing Corporation, Philadelphia
26. Remeli MF, Kiatbodin L, Singh B, Verojporn K, Date A, Akbarzadeh A (2015) Power generation from waste heat using heat pipe and thermoelectric generator. Energy Procedia 75:645–650
27. Rowe D (2006) Thermoelectric waste heat recovery as a renewable energy source. Int J Innov Energy Syst Power 1:13–23
28. Tang ZB, Deng YD, Su CQ, Shuai WW, Xie CJ (2015) A research on thermoelectric generator's electrical performance under temperature mismatch conditions for automotive waste heat recovery system. Case Stud Therm Eng 5:143–150
29. Welty J, Wicks C, Wilson R, Rorrer G (2008) Fundamentals of momentum, heat, and mass transfer, 5th edn. Wiley, Hoboken
30. Wilcox D (1993) Turbulence modeling for CFD, 1st edn. DCW Industries Inc, Delft

Publisher's Note Springer Nature remains neutral with regard to jurisdictional claims in published maps and institutional affiliations.